Long-range superharmonic Josephson current and spin-triplet pairing correlations in a junction with ferromagnetic bilayers

Hao Meng,[1, 2, 3] Jiansheng Wu,[1, *] Xiuqiang Wu,[3] Mengyuan Ren,[4] and Yajie Ren[2]

[1]*Department of Physics, South University of Science and Technology of China, Shenzhen, 518055, China*

[2]*School of Physics and Telecommunication Engineering, Shaanxi University of Technology, Hanzhong 723001, China*

[3]*National Laboratory of Solid State Microstructures and Department of Physics, Nanjing University, Nanjing 210093, China*

[4]*School of material science and technology, Harbin university of science and technology, Harbin 150080, china*

Abstract

The long-range spin-triplet supercurrent transport is an interesting phenomenon in the superconductor/ferromagnet (S/F) heterostructure containing noncollinear magnetic domains. Here we study the long-range superharmonic Josephson current in asymmetric $S/F_1/F_2/S$ junctions. It is demonstrated that this current is induced by spin-triplet pairs $|\uparrow\uparrow\rangle - |\downarrow\downarrow\rangle$ or $|\uparrow\uparrow\rangle + |\downarrow\downarrow\rangle$ in the thick F_1 layer. The magnetic rotation of the particularly thin F_2 layer will not only modulate the amplitude of the superharmonic current but also realise the conversion between $|\uparrow\uparrow\rangle - |\downarrow\downarrow\rangle$ and $|\uparrow\uparrow\rangle + |\downarrow\downarrow\rangle$. Moreover, the critical current shows an oscillatory dependence on thickness and exchange field in the F_2 layer. These effect can be used for engineering cryoelectronic devices manipulating the superharmonic current. In contrast, the critical current declines monotonically with increasing exchange field of the F_1 layer, and if the F_1 layer is converted into half-metal, the long-range supercurrent is prohibited but $|\uparrow\uparrow\rangle$ still exists within the entire F_1 region. This phenomenon contradicts the conventional wisdom and indicates the occurrence of spin and charge separation in present junction, which could lead to useful spintronics devices.

*Electronic address: wu.js@sustc.edu.cn

Superconductor/ferromagnet (S/F) hybrid structure has recently attracted considerable attention because of the potential applications in spintronics and quantum information [1–3] as well as the display of a variety of unusual physical phenomena [4–7]. In general, if a weak F is adjacent to an s-wave S and there is no interfacial spin-flip scattering, the normal Andreev reflection will generate at S/F interfaces. The process involves an electron incident on the S/F interface from the F at energies less than the superconducting energy gap. The incident electron forms a Cooper pair in the S with the retroreflection of a hole of opposite spin to the incident electron. Consequently, the conventional spin-singlet Cooper pair decays at a short range in ferromagnetic region. In $S/F/S$ Josephson junctions with homogeneous magnetization, through the normal Andreev reflection occurring at two S/F interfaces, a Cooper pair is transferred from one S to another, creating a supercurrent flow across the junction [8]. As a consequence of the exchange splitting of the Fermi level of the F, the Cooper pair decay in an oscillatory manner superimposed on an exponential decay in the F. Correspondingly, the Josephson current displays a damped oscillation with increasing the thickness or the exchange field of the F, leading to the appearance of the so-called "0-π transition" [1, 2]. In general, the normal Andreev reflection will be suppressed by the exchange field of the F, so the Josephson current just can transport a short distance.

In contrast, if one insert a thin spin-active F layer with noncollinear magnetization into the S/F interface, it is found that the noncollinear magnetization can lead to a spin-flip scattering, then the reflected hole has the same spin as the incident electron, which is identified as anomalous Andreev reflection. When this reflection takes place at two S/F interfaces, the parallel spin-triplet Cooper pairs $|\uparrow\uparrow\rangle$ are generated in the central F layer and can penetrate into F layer over a long distance unsuppressed by the exchange interaction, so that the proximity effect is enhanced. The induced long-range current manifests itself as a large first harmmonic ($I_1 \gg I_2$) in the spectral decomposition of the Josephson current-phase relation $I(\phi) = I_1 \sin(\phi) + I_2 \sin(2\phi) + \cdots$ [8].

It is worth to point that, if the central F layer is converted into fully spin-polarized half-metal, in which electronic bands exhibit insulating behavior for one spin direction and metallic behavior for the other, the normal Andreev reflection will be inhibited completely due to inability to form a pair in the S and impossibility of single-particle transmission. However, the strength of the anomalous Andreev reflection can not be strongly influenced by the spin-polarization of the F, and the transport processes of $|\uparrow\uparrow\rangle$ (or $|\downarrow\downarrow\rangle$) in the F region

2

will continue to take place. In response, several different inhomogeneous configurations have been proposed for studying such enhanced proximity effect [9–15]. The corresponding experiments have proved these physical process and observed the strong enhancement of the long-range spin-triplet supercurrents [16–21].

Different from the configurations mentioned above, it has proposed a long-range proximity effect develops in highly asymmetric $S/F_1/F_2/S$ junction composed of thick F_1 layer and particularly thin F_2 layer with noncollinear magnetizations at low temperatures [22–24]. This effect arises from two normal Andreev reflections occurred at normal S/F_1 interface and two anomalous Andreev reflections at spin-active F_2/S interface. The long-range spin-triplet correlations in this junction give the dominant second harmonic ($I_2 \gg I_1$) in current-phase relation [23], which is known as superharmonic Josephson current [22]. Recently, Iovan *et al.* [25] experimentally observed the long-range supercurrent through above junction. This second harmonic can be manifested as half-integer Shapiro steps that can be experimentally observed [26], and the two times smaller flux quantum will be obtained, leading to more sensitive quantum interferometers (SQUIDs) [27]. It should be stressed that Refs. [22–24] did not discuss the difference of long-range triplet pairing fashion between asymmetric $S/F_1/F_2/S$ junction and symmetric $S/F_2/F_1/F_2/S$. Moreover, it is high desirable to clarify the effect of the misorientation angle on the triplet pairing correlations in the $S/F_1/F_2/S$ junction, as well as the influence of the thickness and the exchange field in two ferromagnetic layers on the Josephson current and the long-range spin-triplet correlations.

In this work, we study the relation between the long-range superharmonic Josephson current and the spin-triplet pairing correlations in $S/F_1/F_2/S$ junction. It is proposed that the superharmonic Josephson current is induced by the spin-triplet pairs $|\uparrow\uparrow\rangle - |\downarrow\downarrow\rangle$ or $|\uparrow\uparrow\rangle + |\downarrow\downarrow\rangle$ in the long F_1 layer. The variation of the misorientation angle between two magnetizations will not only turn the amplitude of the superharmonic current but also realize the conversion between $|\uparrow\uparrow\rangle - |\downarrow\downarrow\rangle$ and $|\uparrow\uparrow\rangle + |\downarrow\downarrow\rangle$. This can be used to control the superharmic current and the pairing fashion in the F_1 layer through modulating the magnetic structure of the F_2 layer. Besides, the critical current shows an oscillatory dependence on the thickness and exchange field of the highly thin F_2 layer. These effect can be used for engineering cryoelectronic devices manipulating spin-polarized supercurrent. In contrast, the critical current decreases monotonically with increasing exchange field of the F_1 layer. Specifically, if the F_1 layer is converted into half-metal, the long-range Josephson current
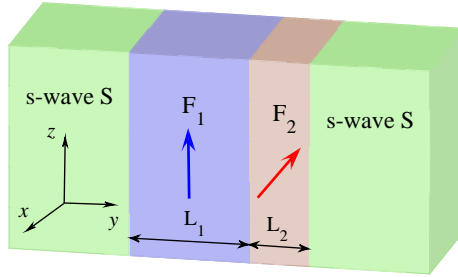
FIG. 1: **Schematic illustration of the $S/F_1/F_2/S$ Josephson junction containing a bilayer ferromagnet.** Thick arrows in F_1 layer and F_2 layer indicate the directions of the magnetic moments. The phase difference between the two s-wave Ss is $\phi = \phi_R - \phi_L$.

will be completely prohibited, but $|\uparrow\uparrow\rangle$ still exist in F_1 region. This phenomenon indicates the occurrence of spin and charge separation in present S/F junction which could lead to useful spintronics devices. These results also contradict the traditional view: the long-range Josephson current is determined by the parallel spin-triplet pairs in the multilayer junction with noncollinear magnetization alignment between ferromagnetic layers. At last, it is also found that the magnetization of the F_2 layer will bring about a same direction magnetization in the F_1 layer on condition that the magnetic moment of the F_1 layer is weak.

To be more precise, we consider the Josephson junction consists of two s-wave superconducting electrodes and ferromagnetic bilayer with noncollinear magnetizations. The schematic picture of the $S/F_1/F_2/S$ device is presented in Fig. 1. One assume that the transport direction is along the y axis, and the system satisfies translational invariance in the x-z plane. The thicknesses of F_1 layer and F_2 layer are L_1 and L_2, respectively. The exchange field $\vec{h}$ due to the ferromagnetic magnetizations in the F_p $(p = 1, 2)$ layer is described by $\vec{h} = h_p(\sin\theta_p \cos\varphi_p, \sin\theta_p \sin\varphi_p, \cos\theta_p)$. Here θ_p is the tilt angle from the z axis, and φ_p is the horizontal angle respect to x axis.

Results

Based on the extended the Blonder-Tinkham-Klapwijk (BTK) approach [28–31], the dc Josephson current in the $S/F_1/F_2/S$ junction can be expressed as follows

$$I_e(\phi) = \frac{k_B T e \Delta}{4\hbar} \sum_{k_\parallel} \sum_{\omega_n} \frac{k_e(\omega_n) + k_h(\omega_n)}{\Omega_n}$$
$$\times \left[\frac{a_1(\omega_n, \phi) - a_2(\omega_n, \phi)}{k_e} + \frac{a_3(\omega_n, \phi) - a_4(\omega_n, \phi)}{k_h} \right], \tag{1}$$

where $\omega_n = \pi k_B T (2n + 1)$ are the Matsubara frequencies with $n = 0, 1, 2, \ldots$ and $\Omega_n = \sqrt{\omega_n^2 + \Delta^2(T)}$. $k_{e(h)}(\omega_n)$ are the perpendicular components of the wave vectors for electron-like (hole-like) quasiparticles in superconducting regions, and $a_j(\omega_n, \phi)$ with $j = 1, 2, 3, 4$ are the scattering coefficients of the normal Andreev reflection under the condition of four different incoming quasiparticles, electron-like quasiparticles (ELQs) and hole-like quasiparticles (HLQs) with spin up and spin down. Then the critical current is derived from $I_c = max_\phi |I_e(\phi)|$.

By applying the Bogoliubov's self-consistent field method [32, 33], the triplet pair amplitudes are defined as follows [34]:

$$f_0(y, t) = \frac{1}{2} \sum_n \sum_{qq'} (u_{nq}^\uparrow v_{nq'}^{\downarrow*} + u_{nq}^\downarrow v_{nq'}^{\uparrow*}) \zeta_q(y) \zeta_{q'}(y) \eta_n(t), \tag{2}$$

$$f_1(y, t) = f_{\uparrow\uparrow}(y, t) - f_{\downarrow\downarrow}(y, t), \tag{3}$$

$$f_2(y, t) = f_{\uparrow\uparrow}(y, t) + f_{\downarrow\downarrow}(y, t), \tag{4}$$

where $\eta_n(t) = \cos(E_n t) - i \sin(E_n t) \tanh(E_n/2k_B T)$, and equal-spin pair amplitude will be denoted by $f_{\alpha\alpha}(y, t) = \frac{1}{2} \sum_n \sum_{qq'} u_{nq}^\alpha v_{nq'}^{\alpha*} \zeta_q(y) \zeta_{q'}(y) \eta_n(t)$. The singlet pair amplitude writes as $f_3(y) = \Delta(y)/g(y)$. In this paper, the singlet and triplet pair amplitudes are all normalized to the value of the singlet pairing amplitude in a bulk superconducting material. The LDOS is given by [34]

$$N(y, \epsilon) = -\sum_n \sum_{qq'} [(u_{nq}^\uparrow u_{nq'}^{\uparrow*} + u_{nq}^\downarrow u_{nq'}^{\downarrow*}) f'(\epsilon - E_n)$$
$$+ (v_{nq}^\uparrow v_{nq'}^{\uparrow*} + v_{nq}^\downarrow v_{nq'}^{\downarrow*}) f'(\epsilon + E_n)] \zeta_q(y) \zeta_{q'}(y), \tag{5}$$

where $f'(\epsilon) = \partial f/\partial \epsilon$ is the derivative of the Fermi function. The LDOS is normalized to unity in the normal state of the S material. In addition, the local magnetic moment in the

$S/F_1/F_2/S$ geometry has three components [34]

$$M_x(y) = -\mu_B \sum_n \sum_{qq'} [(u_{nq}^{\uparrow *} u_{nq'}^{\downarrow} + u_{nq}^{\downarrow *} u_{nq'}^{\uparrow}) f_n$$
$$+ (v_{nq}^{\uparrow} v_{nq'}^{\downarrow *} + v_{nq}^{\downarrow} v_{nq'}^{\uparrow *})(1 - f_n)] \zeta_q(y) \zeta_{q'}(y), \quad (6)$$

$$M_y(y) = i\mu_B \sum_n \sum_{qq'} [(u_{nq}^{\uparrow *} u_{nq'}^{\downarrow} - u_{nq}^{\downarrow *} u_{nq'}^{\uparrow}) f_n$$
$$+ (v_{nq}^{\uparrow} v_{nq'}^{\downarrow *} - v_{nq}^{\downarrow} v_{nq'}^{\uparrow *})(1 - f_n)] \zeta_q(y) \zeta_{q'}(y), \quad (7)$$

$$M_z(y) = -\mu_B \sum_n \sum_{qq'} [(u_{nq}^{\uparrow *} u_{nq'}^{\uparrow} - u_{nq}^{\downarrow *} u_{nq'}^{\downarrow}) f_n$$
$$+ (v_{nq}^{\uparrow} v_{nq'}^{\uparrow *} - v_{nq}^{\downarrow} v_{nq'}^{\downarrow *})(1 - f_n)] \zeta_q(y) \zeta_{q'}(y), \quad (8)$$

where μ_B and f_n are the Bohr magneton and the Fermi function, respectively. It is convenient to normalize these components to $-\mu_B$.
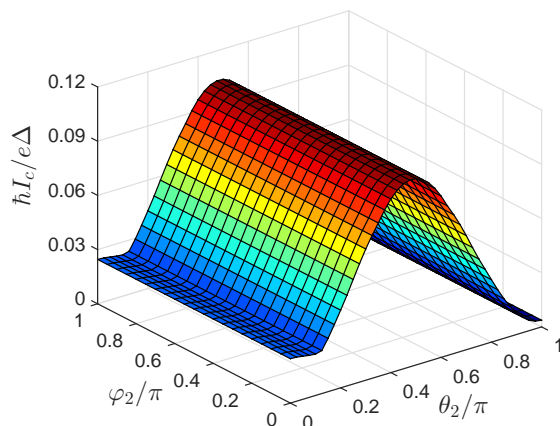

FIG. 2: **Critical current as a function of the orientation angle (θ_2, φ_2) of the F_2 layer.** Here we set $k_F L_1 = 200$, $k_F L_2 = 6$, $h_1/E_F = 0.1$, and $h_2/E_F = 0.16$.

Unless otherwise stated, in BTK approach we use the superconducting gap Δ_0 as the unit of energy. The Fermi energy is $E_F = 1000\Delta_0$, the interface transparency is $Z_{1-4} = 0$ and $T/T_c = 0.1$. We measure all lengths and the exchange field strengths in units of the inverse of the Fermi wave vector k_F and the Fermi energy E_F, respectively. The magnetization in the F_1 layer is fixed along the z direction ($\theta_1 = 0$, $\varphi_1 = 0$), while the F_2 is a free layer in which the magnetization points any direction. In Bogoliubov's self-consistent field method, we consider the low-temperature limit and take $k_F L_{S1} = k_F L_{S2} = 400$, $\omega_D/E_F = 0.1$. The other parameters are the same as the ones mentioned before.

Discussion
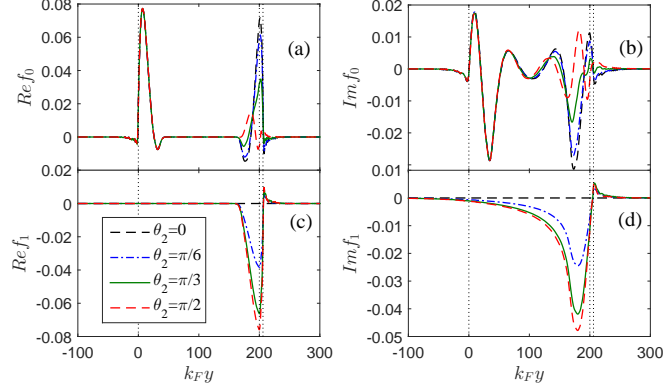
A. Superharmonic currents versus misalignment angle

FIG. 3: **The spin-triplet pair amplitudes f_0 and f_1 plotted as a function of the coordinate $k_F y$ for several values of θ_2 in the case of $\varphi_2 = 0$.** The left panels show the real parts while the right ones show the imaginary parts. The dotted vertical lines represent the location of the S/F_1, F_1/F_2 and F_2/S interfaces. Here $k_F L_1 = 200$, $k_F L_2 = 6$, $h_1/E_F = 0.1$, $h_2/E_F = 0.16$, $\omega_D t = 4$, and $\phi = 0$. All panels utilize the same legend.

From Fig. 2 one can clearly see that the critical current reaches maximum for perpendicular magnetizations ($\theta_2 = \pi/2$) and decreases to minimum as the magnetizations are parallel ($\theta_2 = 0$) or antiparallel ($\theta_2 = \pi$) to each other. However, the variation of the angle φ_2 can not lead to the change of critical current while keeping θ_2 constant. It is known that characteristic variations of the critical current I_c with the misaligned angles (ϑ_2, φ_2) are related to the nature of pairing correlations. Figure 3 shows the spatial distribution of the spin-triplet pair amplitudes for different misalignment angle θ_2 at fixed $\varphi_2 = 0$. It is found that the real part of f_0 and f_1 can not penetrate entire F_1 layer, but their image parts can be distributed throughout this region. With increasing θ_2, the left parts of $Im f_0$ are almost unchanged, however, their right parts gradually decrease. Correspondingly, the amplitudes of $Im f_1$ increase and turn to maximum at $\theta_2 = \pi/2$. The main reason is because the x-projection of misaligned magnetic moment in the F_2 layer can generate two separate effects: spin-mixing and spin-flip scattering process [9]. The former will result a mixture of singlet pairs and triplet pairs with zero spin projection $(|\uparrow\downarrow\rangle - |\downarrow\uparrow\rangle)_x \cos(Q \cdot R) + i(|\uparrow\downarrow\rangle + |\downarrow\uparrow\rangle)_x \sin(Q \cdot R)$, where

$Q \simeq 2h/\hbar v_F$, v_F is the Fermi velocity and R is the distance from the F_2/S interface. The latter can convert $(|\uparrow\downarrow\rangle + |\downarrow\uparrow\rangle)_x$ into the parallel spin-triplet pairs $(|\uparrow\uparrow\rangle - |\downarrow\downarrow\rangle)_z$ [3]. These parallel spin pairs will penetrate coherently over a long distance into the F_1 layer. So the transport of $(|\uparrow\uparrow\rangle - |\downarrow\downarrow\rangle)_z$ can make a significant contribution to superharmonic Josephson current. Meanwhile, the period of this current becomes π and satisfies the second harmonic current-phase relation $I_e(\phi) \propto \sin 2\phi$ [22, 24]. By contrast, in the Josephson junction with ferromagnetic trilayer only spin-triplet pairs $|\uparrow\uparrow\rangle$ (or $|\downarrow\downarrow\rangle$) can transmit in central ferromagnetic layer, which provide the main contribution to the long-range first harmonic current [35].
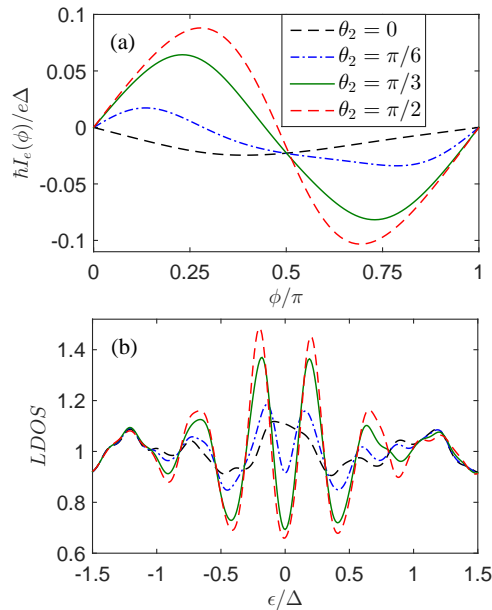

FIG. 4: (a) the Josephson current-phase relation $I_e(\phi)$ for four values of the relative angle θ_2 between magnetizations. (b) The normalized LDOS in the F_1 layer ($k_F y = 180$) plotted versus the dimensionless energy ϵ/Δ for different θ_2, and the results are calculated at $k_B T = 0.0008$. Other parameters are the same as in Fig. 3.

As plotted in Fig. 4, in the case of collinear orientation of magnetizations ($\theta_2 = 0$), the current $I_e(\phi)$ is weak enough and present a first harmonic feature. At this time, the long-range spin-triplet pairs $|\uparrow\uparrow\rangle - |\downarrow\downarrow\rangle$ are absent, so the LDOS in the F_1 layer is almost equal to its normal metal value. With increasing θ_2, the magnitude of the second harmonic current is enhanced by the increased number of $|\uparrow\uparrow\rangle - |\downarrow\downarrow\rangle$. Specifically, for orthogonal magnetizations ($\theta_2 = \pi/2$), the second harmonic current grows big enough. Correspondingly, the LDOS is significantly enhanced with two distinguishable peaks. Moreover, the spatial profile of

the local magnetic moments are plotted for several values of θ_2 in Fig. 5. What's most interesting is that the component M_x grows very quickly in the F_2 region with increasing θ_2, and also displays the penetration of the same component into the F_1 region. The induced M_x in the F_1 region tends to not only change magnitude as a function of position, but it also rotates direction. However, the component M_z in the F_2 region will gradually decrease with θ_2 and remains almost unchanged in F_1 region.
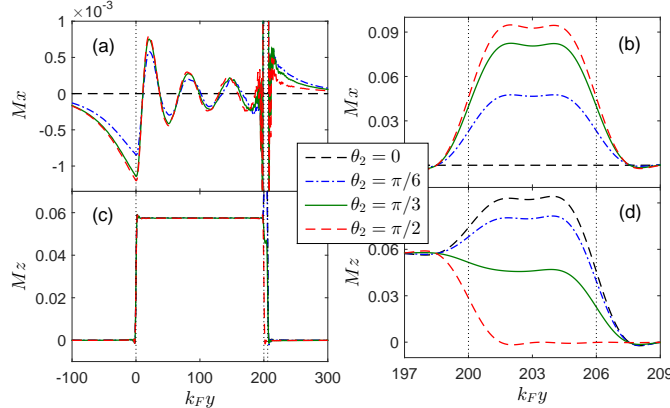

FIG. 5: **The x (top panels) and z components (bottom panels) of the local magnetic moment plotted as a function of the coordinate $k_F y$ for different θ_2.** The left panels show the behaviours over the extended F_1 regions while the right ones show the detailed behaviours in the F_2 layer. Other parameters are the same as in Fig. 3.

As stated above, the variation of the horizontal angle φ_2 can not influence the Josephson current as the tilt angle θ_2 has a fixed value. However, the change of φ_2 will induced a conversion of pairing fashion in the F_1 region. As shown in Fig. 6, on the condition of $\theta_2 = \pi/2$, Imf_1 decrease gradually from a finite value to zero with increasing φ_2, but Ref_2 exhibit the opposite characteristics. These phenomena can be explained as follows: since the magnetic direction of the F_2 layer is oriented along the x axis ($\theta_2 = \pi/2$, $\varphi_2 = 0$), $(|\uparrow\downarrow\rangle + |\downarrow\uparrow\rangle)_x$ in the F_2 layer can be converted into $(|\uparrow\uparrow\rangle - |\downarrow\downarrow\rangle)_z$ in the F_1 layer. In contrast, if the magnetic moment of the F_2 layer is along y axis ($\theta_2 = \pi/2$, $\varphi_2 = \pi/2$), $(|\uparrow\downarrow\rangle + |\downarrow\uparrow\rangle)_y$ will be transformed into $i(|\uparrow\uparrow\rangle + |\downarrow\downarrow\rangle)_z$, which can also penetrate into the F_1 region a long distance and make a major contribution to the second harmonic current. At the same time, when the magnetization direction of the F_2 layer rotate from the x axis to the y axis, the induced magnetic moment in the F_1 layer would correspondingly turn from M_x to M_y, as

9

seen in Fig. 7. In what follows, we focus on the dependence of the critical current on the thickness and exchange fields of two ferromagnetic layers under the condition of $\varphi_2 = 0$.
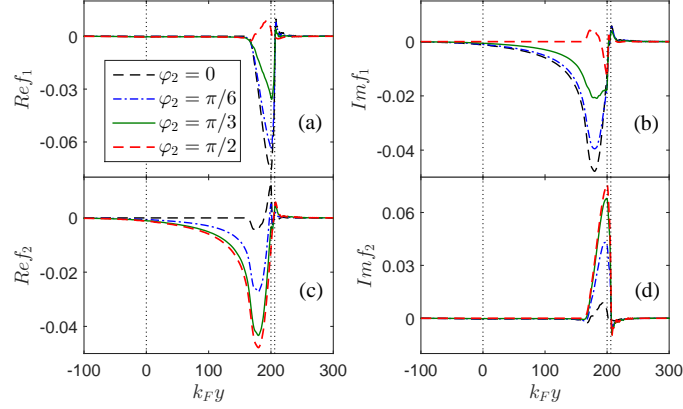

FIG. 6: **The spin-triplet pair amplitudes f_1 [(a) and (b)] and f_2 [(c) and (d)] plotted as a function of the coordinate $k_F y$ for several values of φ_2 in the case of $\theta_2 = \pi/2$.** The left panels [(a) and (c)] show the real parts while the right ones [(b) and (d)] show the imaginary parts. Other parameters are the same as in Fig. 3.
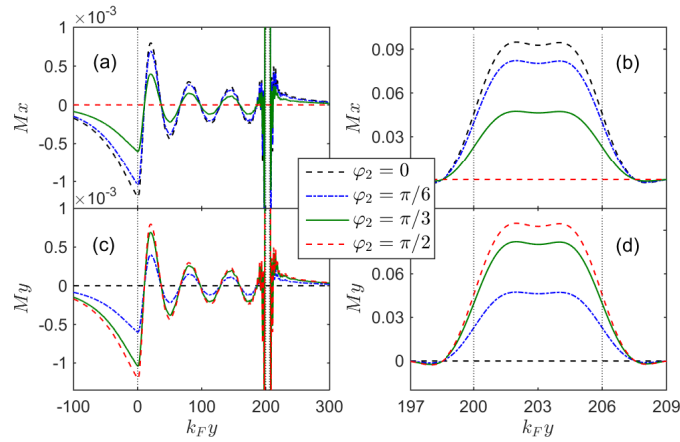

FIG. 7: **The x (top panels) and y components (bottom panels) of the local magnetic moment plotted as a function of the coordinate $k_F y$ for different φ_2.** The left panels show the behaviours over the extended F_1 region while the right ones show the detailed behaviours in the F_2 region. Other parameters are the same as in Fig. 3.

B. Superharmonic currents versus thickness and exchange field of the spin-active F_2 layer

Figure 8 shows the dependence of the critical current I_c on the length $k_F L_2$ and exchange field h_2/E_F for different misalignment angle θ_2 when the F_1 layer has fixed values $h_1/E_F = 0.1$ and $k_F L_1 = 200$. One can see that I_c is sufficiently weak and decays in an oscillatory manner in parallel ($\theta_2 = 0$) and antiparallel ($\theta_2 = \pi$) alignments of the magnetizations. This is because the exchange field in the F_2 layer induces a splitting of the energy bands for spin up and spin down. This effect can make I_c oscillate with a period $2\pi\xi_F$ and simultaneously decay exponentially on the length scale of ξ_F [1]. Here, ξ_F is the magnetic coherence length. In this case, only the spin-singlet pairs $|\uparrow\downarrow\rangle - |\downarrow\uparrow\rangle$ and spin-triplet pairs $|\uparrow\downarrow\rangle + |\downarrow\uparrow\rangle$ exist in the ferromagnetic layer. These two types of pairs can be suppressed by the exchange field of ferromagnetic layer and mainly provide the contribution to the first harmonic current.
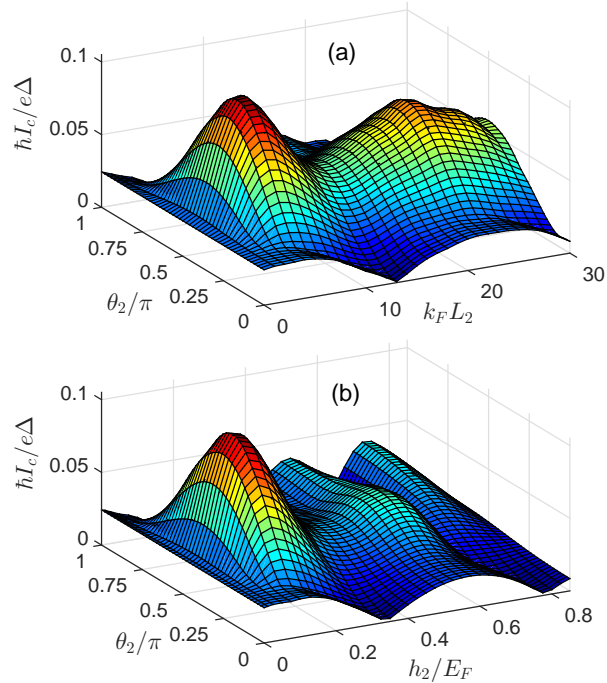

FIG. 8: Critical current (a) as a function of $k_F L_2$ and θ_2 for $h_2/E_F = 0.16$, and (b) as a function of h_2/E_F and θ_2 for $k_F L_2 = 6$. We set $k_F L_1 = 200$, $h_1/E_F = 0.1$, and $\varphi_2 = 0$.

On the other hand, if the orientations of the magnetic moments are perpendicular to each other ($\theta_2 = \pi/2$), I_c also displays the oscillated behaviour with increasing $k_F L_2$, but its

order of magnitude is larger than for collinear magnetizations. This characteristic behaviour can be attributed to the spatial oscillations of $|\uparrow\downarrow\rangle+|\downarrow\uparrow\rangle$ in the F_2 region with period $Q \cdot R$. It is well known that the Cooper pair in the F_2 layer will acquire a total momentum Q because of the spin splitting of the energy bands. As described in Ref. [36], for a fixed Q the amplitude of $|\uparrow\downarrow\rangle+|\downarrow\uparrow\rangle$ will vary with the length R $(= k_F L_2)$ of the F_2 layer. As a result, the oscillated $|\uparrow\downarrow\rangle+|\downarrow\uparrow\rangle$ can be converted into $|\uparrow\uparrow\rangle-|\downarrow\downarrow\rangle$ in the F_1 layer by the spin-flip scattering, and then $|\uparrow\uparrow\rangle-|\downarrow\downarrow\rangle$ can propagate over long distance in the F_1 layer and lead to the enhanced superharmonic current. Similarly, if one fixes $k_F L_2$ and changes the h_2/E_F, the same features about the critical current can be obtained (see Fig. 8 (b)). It is worth mentioning that this oscillatory behaviour could be different from the oscillation of the critical current with the thickness of F_2 layer in $S/F_2/F_1/F_2/S$ junction [36], because the supercurrent in the central F_1 layer derives from the contribution of $|\uparrow\uparrow\rangle$ and manifests itself as a dominant first harmonic in the Josephson current-phase relation.
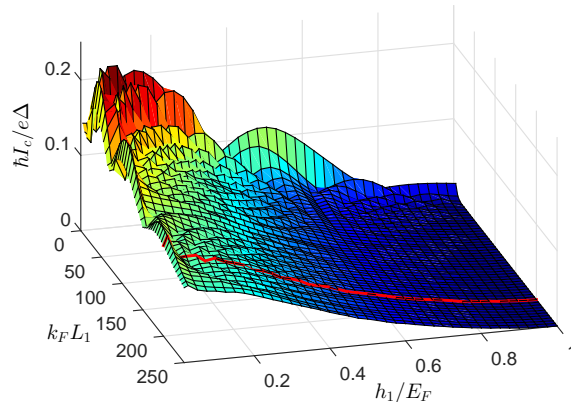

FIG. 9: **Critical current as a function of h_1/E_F and $k_F L_1$.** We set $k_F L_2 = 6$, $h_2/E_F = 0.16$, $\theta_2 = \pi/2$, and $\varphi_2 = 0$.

C. Superharmonic currents versus length and exchange field of the long F_1 layers

In Fig. 9 the dependence of the critical current I_c on exchange field h_1/E_F and length $k_F L_1$ are plotted for $\theta_2 = \pi/2$. Compared with the Josephson junctions with homogeneous magnetization, I_c in this asymmetric junctions decreases slowly with increasing $k_F L_1$ on the weak or moderate exchange fields. This feature illustrates that $|\uparrow\uparrow\rangle-|\downarrow\downarrow\rangle$ will propagate

coherently over long distances in the F_1 layer. Furthermore, I_c are almost monotonically decreasing with h_1/E_F for various $k_F L_1$ and will be prohibited completely at $h_1/E_F = 1$. It indicates that the superharmonic current will be suppressed by the exchange field of the F_1 layer. This phenomenon is clearly different from the first harmonic current in the half-metal Josephson junction with interface spin-flip scattering [9, 16], because the first harmonic current induced by $|\uparrow\uparrow\rangle$ can not be suppressed by the exchange splitting.
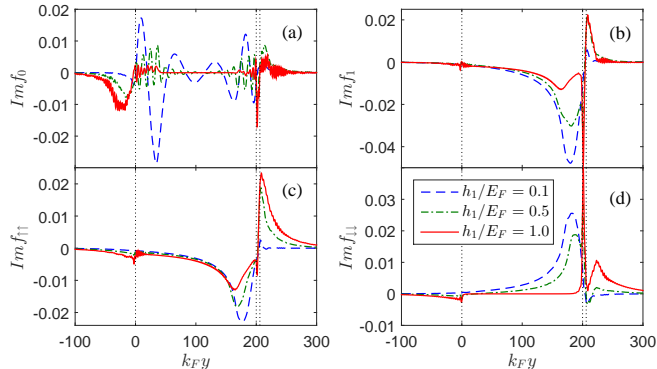

FIG. 10: The imaginary parts of f_0 (a), f_1 (b), $f_{\uparrow\uparrow}$ (c) and $f_{\downarrow\downarrow}$ (d) plotted as a function of the coordinate $k_F y$ for several h_1/E_F. We set $k_F L_1 = 200$, $k_F L_2 = 6$, $h_2/E_F = 0.16$, $\theta_2 = \pi/2$, $\varphi_2 = 0$, $\omega_D t = 4$, and $\phi = 0$.

In order to clearly explain the contribution of the spin-triplet pairs to the superharmonic current, we choose a fixed length $k_F L_1 = 200$ for discussion, as illustrated by the red line in Fig. 9. Under such conditions, we plot the distribution of the spin-triplet pairing functions f_0, f_1, $f_{\uparrow\uparrow}$ and $f_{\downarrow\downarrow}$ for three exchange fields $h_1/E_F = 0.1$, 0.5, and 1.0 in Fig. 10. With increasing h_1/E_F, the magnitude of f_0 and f_1 in the F_1 region are all reduced and f_0 drops to zero at $h_1/E_F = 1$. The reason can be summarized as follows: for weak exchange field $h_1/E_F = 0.1$ the triplet correlations $f_{\uparrow\uparrow}$ and $f_{\downarrow\downarrow}$ will generate in the F_2 region and then combine into f_1 in the F_1 region. f_1 decay spatially with approaching the S/F_1 interface due to the fact that the pairs $|\uparrow\uparrow\rangle$ and $|\downarrow\downarrow\rangle$ are recombined into the pairs $|\uparrow\downarrow\rangle$ and $|\downarrow\uparrow\rangle$ by the normal Andreev reflections. For $h_1/E_F = 0.5$, $f_{\uparrow\uparrow}$ and $f_{\downarrow\downarrow}$ near the F_2/S interface are both restrained. By contrast, $f_{\uparrow\uparrow}$ adjacent to the S/F_1 interface increases instead. Moreover, because $f_{\downarrow\downarrow}$ on the left side of F_1 layer is suppressed, the recombination effect at the S/F_1 interface becomes weakened, in which case the superharmonic current will decrease. For a fully spin-polarized half-metal ($h_1/E_F = 1$), Fig. 10(d) shows that $f_{\downarrow\downarrow}$ will be completely

13

suppressed, but $f_{\uparrow\uparrow}$ does not vanish and it's magnitude seems to be a slight increase in the vicinity of the S/F_1 interface (see Fig. 10(c)). These characters can be attributed to the contributions from two important phenomena taking place at the S/F_1 interface: normal Andreev reflections and normal reflections, as shown in Fig. 11 (a) and (b), respectively.
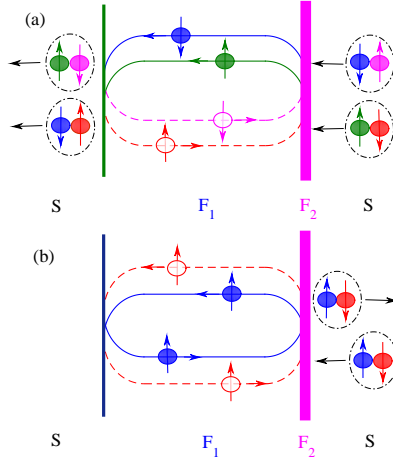

FIG. 11: **Two types of transference about the pairs of correlated electrons and holes.** (a) The first one consists of two normal Andreev reflections occurred at S/F_1 interface and two anomalous Andreev reflections at F_2/S interface in the case of weak exchange field in the F_1 layer. (b) The second one consists of two normal reflections at S/F_1 interface and two anomalous Andreev reflections at F_2/S interface while the F_1 layer is converted into half-metal.

If the exchange field h_1/E_F is weak enough, the normal Andreev reflections will mainly occur at the S/F_1 interface, which provide the main contribution to I_c. In this case, the number of the pairs $|\uparrow\uparrow\rangle$ approximately equal to $|\downarrow\downarrow\rangle$, and then $|\uparrow\uparrow\rangle$ and $|\downarrow\downarrow\rangle$ can combine into $|\uparrow\uparrow\rangle - |\downarrow\downarrow\rangle$. Subsequently, $|\uparrow\uparrow\rangle - |\downarrow\downarrow\rangle$ can be converted into $|\uparrow\downarrow\rangle - |\downarrow\uparrow\rangle$ in the left S. With increasing h_1/E_F, the normal Andreev reflections are gradually being replaced by the normal reflections, and the difference in the number of $|\uparrow\uparrow\rangle$ and $|\downarrow\downarrow\rangle$ will enlarge simultaneously. As a result, the transition from $|\uparrow\uparrow\rangle - |\downarrow\downarrow\rangle$ to $|\uparrow\downarrow\rangle - |\downarrow\uparrow\rangle$ occurred at the S/F_1 interface will be weakened. In the fully spin-polarized case ($h_1/E_F = 1$) the absence of the spin down electrons makes it impossible to generate the normal Andreev reflections at S/F_1 interface, and therefore the Josephson current is completely suppressed but $|\uparrow\uparrow\rangle$ still exist. As depicted in Fig. 11 (b), the electron transfer process is analogous to the unconventional equal-spin Andreev-reflection process reported in Ref. [37]. Look at the whole picture, it is easy to

understand the above process: $|\uparrow\downarrow\rangle$ injecting from the right S is converted into $|\uparrow\uparrow\rangle$ in the F_1 layer, and $|\uparrow\uparrow\rangle$ will be consequently reflected normally back as $|\uparrow\uparrow\rangle$ at the S/F_1 interface. Then $|\uparrow\uparrow\rangle$ is transformed into $|\uparrow\downarrow\rangle$ by the spin-flip scattering of the F_2 layer. At last, $|\uparrow\downarrow\rangle$ transports to the right S. In the whole process, none of Coopers can penetrate into the left S, so the Josephson current would be suppressed completely.
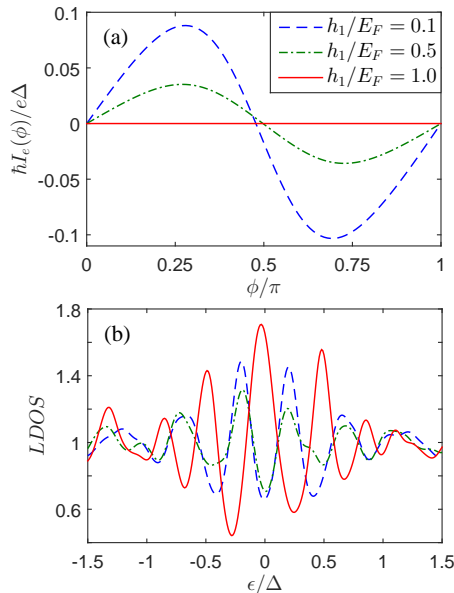

FIG. 12: (a) the Josephson current-phase relation $I_e(\phi)$ for different h_1/E_F. (b) The normalized LDOS in the F_1 layer ($k_F y = 180$) plotted versus the dimensionless energy ϵ/Δ, and the results are calculated at $k_B T = 0.0008$. Other parameters are the same as in Fig. 10.

In order to facilitate the experimental observations for the future, we plot the current-phase relation and the LDOS in the F_1 layer at three points $h_1/E_F = 0.1$, 0.5 and 1.0 in Fig. 12. With increasing h_1/E_F, the superharmonic current $I_e(\phi)$ decreases and two distinguishable peaks in the LDOS will become weak correspondingly. It's particularly noteworthy that if $h_1/E_F = 1$ Josephson current was completely suppressed but the LDOS displays a sharp zero energy conductance peak which marks the presence of $|\uparrow\uparrow\rangle$. It can be measured in principle by STM experiments. And this feature is different from the conventional views: (i) The long-range triplet Josephson current is proportional to the parallel spin-triplet pairs $|\uparrow\uparrow\rangle$ or $|\downarrow\downarrow\rangle$. (ii) If the long-range triplet supercurrent pass through the Josephson junction, there will present the zero energy conductance peak in the LDOS of F. Finally, we discuss the influence of h_1/E_F on the local magnetic moment. As can be seen from Fig. 13, in the

F_1 region M_z will grow with the increase of h_1/E_F, but the induced M_x could be suppressed. For $h_1/E_F = 1$, the M_z reaches maximum but M_x will disappear. By contrast, M_x in the F_2 region hardly changes with h_1/E_F, and M_z will partly permeate into the F_2 layer.
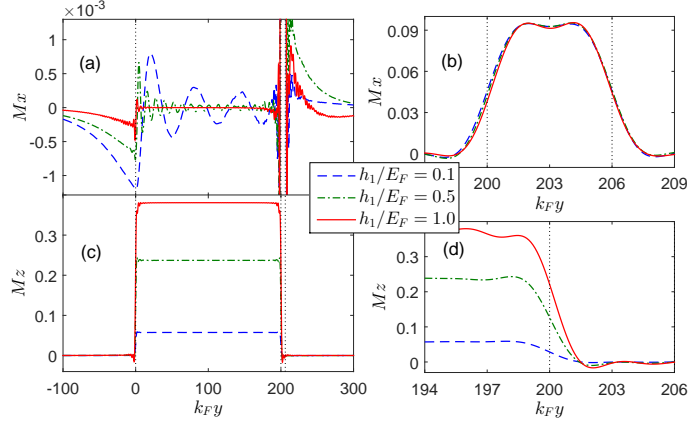

FIG. 13: **The x (top panels) and z components (bottom panels) of the local magnetic moment plotted as a function of the coordinate $k_F y$ for different h_1/E_F.** The left panels show the behaviours over the extended F_1 region while the right ones show the detailed behaviours in the F_2 layer. Other parameters are the same as in Fig. 10.

To summarize, we have studied the long-range superharmonic Josephson current and the spin-triplet pairing correlations in the asymmetric $S/F_1/F_2/S$ junction. We have shown that the superharmonic current was induced by the spin-triplet pairs $|\uparrow\uparrow\rangle - |\downarrow\downarrow\rangle$ or $|\uparrow\uparrow\rangle + |\downarrow\downarrow\rangle$ in the long F_1 layer. The rotation of the magnetic moment in the thin spin-active F_2 layer will not only modulate the amplitude of the superharmonic current through the junctions, but also realize the conversion from $|\uparrow\uparrow\rangle - |\downarrow\downarrow\rangle$ to $|\uparrow\uparrow\rangle + |\downarrow\downarrow\rangle$ in the F_1 layer. Besides, the critical current oscillates with the length and exchange field in the F_2 layer. These features provide an efficient way to control the superharmonic current and the spin-triplet pairing fashion by changing the magnetic moment of the F_2 layer. Specifically, the critical current almost decreases monotonically with the exchange field of the F_1 layer, and if the F_1 layer is converted into half-metal, the Josephson current disappear completely but the spin-triplet pairs $|\uparrow\uparrow\rangle$ still exist within the entire F_1 layer. This behavior is different from the conventional view about the relationship between the long-range current and the parallel spin-triplet pairs in the junctions with ferromagnetic trilayers. These results therefore indicated that the spin and charge degrees of the freedom can be separated in practice in the junction with ferro-

magnetic bilayers, and suggested the promising potential of these junctions for spintronics applications.

Methods

The BCS mean-field effective Hamiltonian is given by [1, 32]

$$H_{eff} = \int d\vec{r}\{\sum_{\alpha,\beta}\psi_\alpha^\dagger(\vec{r})[H_e(\hat{\mathbf{1}})_{\alpha\beta} - (\vec{h}\cdot\vec{\sigma})_{\alpha\beta}]\psi_\beta(\vec{r})$$
$$+ \frac{1}{2}[\sum_{\alpha,\beta}(i\sigma_y)_{\alpha\beta}\Delta(\vec{r})\psi_\alpha^\dagger(\vec{r})\psi_\beta^\dagger(\vec{r}) + h.c.]\},$$

(9)

where $H_e = -\hbar^2\nabla^2/2m - E_F$ is the single-particle Hamiltonian, $\psi_\alpha^\dagger(\vec{r})$ and $\psi_\alpha(\vec{r})$ are creation and annihilation operators with spin α. $\hat{\sigma}$ and E_F denote Pauli matrix and the Fermi energy, respectively. $\Delta(\vec{r}) = \Delta(T)[e^{i\phi_L}\Theta(-y) + e^{i\phi_R}\Theta(y - L_F)]$ describes the superconducting pair potential with $L_F = L_1 + L_2$. Here $\Delta(T)$ accounts for the temperature-dependent energy gap. It satisfies the BCS relation $\Delta(T) = \Delta_0\tanh(1.74\sqrt{T_c/T - 1})$, where Δ_0 is the energy gap at zero temperature and T_c is the superconducting critical temperature. $\Theta(y)$ is the unit step function and $\phi_{L(R)}$ is the phase of the left (right) S.

By making use of the Bogoliubov transformation $\psi_\alpha(y) = \sum_n[u_{n\alpha}(y)\hat{\gamma}_n + v_{n\alpha}^*(y)\hat{\gamma}_n^\dagger]$ and the anticommutation relations of the quasiparticle annihilation and creation operators $\hat{\gamma}_n$ and $\hat{\gamma}_n^\dagger$, we have the Bogoliubov-de Gennes (BdG) equation [1, 32]

$$\begin{pmatrix} H_e - h_z & -h_x + ih_y & 0 & \Delta(y) \\ -h_x - ih_y & H_e + h_z & -\Delta(y) & 0 \\ 0 & -\Delta^*(y) & -H_e + h_z & h_x + ih_y \\ \Delta^*(y) & 0 & h_x - ih_y & -H_e - h_z \end{pmatrix}\begin{pmatrix} u_\uparrow(y) \\ u_\downarrow(y) \\ v_\uparrow(y) \\ v_\downarrow(y) \end{pmatrix} = \begin{pmatrix} u_\uparrow(y) \\ u_\downarrow(y) \\ v_\uparrow(y) \\ v_\downarrow(y) \end{pmatrix}.$$

(10)

Blonder-Tinkham-Klapwijk approach The BdG equation (10) can be solved for each superconducting electrode and each F layer, respectively. For an incident spin up electron in the left S, the wave functions in the S leads and the F_p layer are

$$\Psi_L^S(y) = (u\hat{e}_1 e^{\frac{i\phi_L}{2}} + v\hat{e}_4 e^{-\frac{i\phi_L}{2}})e^{ik_e y}$$
$$+ [(a_1\hat{e}_1 - a_1'\hat{e}_2)ve^{\frac{i\phi_L}{2}} + (a_1\hat{e}_4 + a_1'\hat{e}_3)ue^{-\frac{i\phi_L}{2}}]e^{ik_h y}$$
$$+ [(b_1\hat{e}_1 + b_1'\hat{e}_2)ue^{\frac{i\phi_L}{2}} + (b_1\hat{e}_4 - b_1'\hat{e}_3)ve^{-\frac{i\phi_L}{2}}]e^{-ik_e y},$$

(11)

$$\Psi_p^F(y) = T_p\{[f_{p1}e^{ik_{Fp}^{e\uparrow}y} + f_{p2}e^{-ik_{Fp}^{e\uparrow}y}]\hat{e}_1 + [f_{p3}e^{ik_{Fp}^{e\downarrow}y}$$
$$+ f_{p4}e^{-ik_{Fp}^{e\downarrow}y}]\hat{e}_2 + [f_{p5}e^{-ik_{Fp}^{h\uparrow}y} + f_{p6}e^{ik_{Fp}^{h\uparrow}y}]\hat{e}_3 \qquad (12)$$
$$+ [f_{p7}e^{-ik_{Fp}^{h\downarrow}y} + f_{p8}e^{ik_{Fp}^{h\downarrow}y}]\hat{e}_4\},$$

$$\Psi_R^S(y) = [(c_1\hat{e}_1 + c_1'\hat{e}_2)ue^{\frac{i\phi_R}{2}} + (c_1\hat{e}_4 - c_1'\hat{e}_3)ve^{-\frac{i\phi_R}{2}}]e^{ik_e y}$$
$$+ [(d_1\hat{e}_1 - d_1'\hat{e}_2)ve^{\frac{i\phi_R}{2}} + (d_1\hat{e}_4 + d_1'\hat{e}_3)ue^{-\frac{i\phi_R}{2}}]e^{-ik_h y}. \qquad (13)$$

Here $\hat{e}_1 = [1,0,0,0]^T$, $\hat{e}_2 = [0,1,0,0]^T$, $\hat{e}_3 = [0,0,1,0]^T$, $\hat{e}_4 = [0,0,0,1]^T$ are basis wave functions. Quasiparticle amplitudes are defined as $u = \sqrt{(1 + \Omega/E)/2}$ and $v = \sqrt{(1 - \Omega/E)/2}$ with $\Omega = \sqrt{E^2 - \Delta^2}$. The perpendicular components of the ELQs (HLQs) wave vector in S leads and F_p layer are given by $k_{e(h)} = \sqrt{2m[E_F + (-)\Omega]/\hbar^2 - k_\parallel^2}$ and $k_{Fp}^{e(h)\alpha} = \sqrt{2m[E_F + (-)E + \rho_\alpha h_p]/\hbar^2 - k_\parallel^2}$ with $\rho_{\uparrow(\downarrow)} = 1(-1)$, respectively. It is worthy to note that the parallel component $k_\parallel$ is conserved in transport processes of the quasiparticles. The matrix can be defined as [38]

$$T_p = \begin{pmatrix} \cos\frac{\theta_p}{2}e^{-i\varphi_p} & -\sin\frac{\theta_p}{2}e^{-i\varphi_p} & 0 & 0 \\ \sin\frac{\theta_p}{2} & \cos\frac{\theta_p}{2} & 0 & 0 \\ 0 & 0 & \cos\frac{\theta_p}{2}e^{i\varphi_p} & -\sin\frac{\theta_p}{2}e^{i\varphi_p} \\ 0 & 0 & \sin\frac{\theta_p}{2} & \cos\frac{\theta_p}{2} \end{pmatrix}. \qquad (14)$$

The coefficients b_1, b_1', a_1' and a_1 describe normal reflection, the normal reflection with spin-flip, anomalous Andreev reflection, and normal Andreev reflection, respectively. f_{pr} ($r = 1$–8) are quasiparticles wave function amplitudes in the F_p layer. Likewise, c_1, d_1, c_1' and d_1' are the quasiparticles transmission amplitudes in the right superconducting electrode. All scattering coefficients can be determined by solving the continuity conditions of the wave function and its derivative at the interface

$$\Psi_L^S(y_1) = \Psi_1^F(y_1), \partial_y[\psi_1^F - \psi_L^S]|_{y_1} = 2k_F Z_1 \psi_1^F(y_1);$$
$$\Psi_1^F(y_2) = \Psi_2^F(y_2), \partial_y[\psi_2^F - \psi_1^F]|_{y_2} = 2k_F Z_2 \psi_2^F(y_2); \qquad (15)$$
$$\Psi_2^F(y_3) = \Psi_R^S(y_3), \partial_y[\psi_R^S - \psi_2^F]|_{y_3} = 2k_F Z_3 \psi_R^S(y_3).$$

Here Z_1–Z_3 are dimensionless parameters describing the magnitude of the interfacial resistances. $y_{1-3} = 0, L_1, L_F$ are local coordinate values at the interfaces, and $k_F = \sqrt{2mE_F}$ is the Fermi wave vector. From the boundary conditions, we obtain a system of linear equations that yield the scattering coefficients.

Bogoliubov's self-consistent field method We put the $S/F_1/F_2/S$ junction in a one-dimensional square potential well with infinitely high walls, then the eigenvalues and eigenvectors of the BdG equation (10) have the following changes: $E \to E_n$ and $[u_\uparrow(y), u_\downarrow(y), v_\uparrow(y), v_\downarrow(y)]^T \to [u_{n\uparrow}(y), u_{n\downarrow}(y), v_{n\uparrow}(y), v_{n\downarrow}(y)]^T$. Accordingly, the corresponding quasiparticle amplitudes can be expanded in terms of a set of basis vectors of the stationary states [39], $u_{n\alpha}(y){=}\sum_q u_{nq}^\alpha \zeta_q(y)$ and $v_{n\alpha}(y) = \sum_q v_{nq}^\alpha \zeta_q(y)$ with $\zeta_q(y) = \sqrt{2/L}\sin(q\pi y/L)$. Here, q is a positive integer and $L = L_{S1} + L_F + L_{S2}$. L_{S1} and L_{S2} are the thicknesses of the left and right superconducting electrodes, respectively. The superconducting pair potential in the BdG equation (10) is determined by the self-consistency condition [32]

$$\Delta(y) = \frac{g(y)}{2} \sideset{}{'}\sum_{n} \sum_{qq'} (u_{nq}^\uparrow v_{nq'}^{\downarrow *} - u_{nq}^\downarrow v_{nq'}^{\uparrow *})\zeta_q(y)\zeta_{q'}(y)\tanh(\frac{E_n}{2k_B T}), \tag{16}$$

where the primed sum of E_n is over eigenstates corresponding to positive energies smaller than or equal to the Debye cutoff energy ω_D, and the superconducting coupling parameter $g(y)$ is a constant in the superconducting regions and zero elsewhere. Iterations are performed until self-consistency is reached, starting from the stepwise approximation for the pair potential.

[1] Buzdin, A. I. Proximity effects in superconductor-ferromagnet heterostructures. *Rev. Mod. Phys.* **77**, 935 (2005).

[2] Bergeret, F. S., Volkov, A. F. & Efetov, K. B. Odd triplet superconductivity and related phenomena in superconductor-ferromagnet structures. *Rev. Mod. Phys.* **77**, 1321 (2005).

[3] Eschrig, M. Spin-polarized supercurrents for spintronics. *Phys. Today* **64**(1), 43 (2011).

[4] Nussinov, Z., Shnirman, A., Arovas, D. P., Balatsky, A. V. & Zhu, J. X. Spin and spin-wave dynamics in Josephson junctions. *Phys. Rev. B* **71**, 214520 (2005).

[5] Sperstad, I. B., Linder, J. & Sudbø, A. Josephson current in diffusive multilayer superconductor/ferromagnet/superconductor junctions. *Phys. Rev. B* **78**, 104509 (2008).

[6] Colci, M., Sun, K., Shah, N., Vishveshwara, S. & Harlingen, D. J. V. Anomalous polarization-dependent transport in nanoscale double-barrier superconductor/ferromagnet/superconductor junctions. *Phys. Rev. B* **85**, 180512(R) (2012).

[7] Sun, K., Shah, N. & Vishveshwara, S. Transport in multiterminal superconductor/ferromagnet junctions having spin-dependent interfaces. *Phys. Rev. B* **87**, 054509 (2013).

[8] Golubov, A. A., Kupriyanov, M. Y. & Ilichev, E. The current-phase relation in Josephson junctions. *Rev. Mod. Phys.* **76**, 411 (2004).

[9] Eschrig, M., Kopu, J., Cuevas, J. C. & Schön G. Theory of Half-Metal/Superconductor Heterostructures. *Phys. Rev. Lett.* **90**, 137003 (2003); Eschrig, M. & Lofwander, T. Triplet supercurrents in clean and disordered half-metallic ferromagnets. *Nature Physics* **4**, 138 (2008).

[10] Bergeret, F. S., Volkov, A. F. & Efetov, K. B. Long-Range Proximity Effects in Superconductor-Ferromagnet Structures. *Phys. Rev. Lett.* **86**, 4096 (2001).

[11] Volkov, A. F., Bergeret, F. S. & Efetov, K. B. Odd Triplet Superconductivity in Superconductor-Ferromagnet Multilayered Structures. *Phys. Rev. Lett.* **90**, 117006 (2003).

[12] Asano, Y., Tanaka, Y. & Golubov, A. A. Josephson Effect due to Odd-Frequency Pairs in Diffusive Half Metals. *Phys. Rev. Lett.* **98**, 107002 (2007); Asano, Y., Sawa, Y., Tanaka, Y. & Golubov, A. A. Odd-frequency pairs and Josephson current through a strong ferromagnet. *Phys. Rev. B* **76**, 224525 (2007).

[13] Volkov, A. F. & Efetov, K. B. Odd spin-triplet superconductivity in a multilayered superconductor-ferromagnet Josephson junction. *Phys. Rev. B* **81**, 144522 (2010).

[14] Alidoust, M., Linder, J., Rashedi, G., Yokoyama, T. & Sudbo, A. Spin-polarized Josephson current in superconductor/ferromagnet/superconductor junctions with inhomogeneous magnetization, *Phys. Rev. B* **81**, 014512 (2010).

[15] Halasz, G. B., Blamire, M. G. & Robinson, J. W. A. Magnetic-coupling-dependent spin-triplet supercurrents in helimagnet/ferromagnet Josephson junctions. *Phys. Rev. B* **84**, 024517 (2011).

[16] Keizer, R. S., Goennenwein, S. T. B., Klapwijk, T. M., Miao, G., Xiao, G. & Gupta A. A spin triplet supercurrent through the half-metallic ferromagnet CrO_2. *Nature* **439**, 825 (2006).

[17] Anwar, M. S., Czeschka, F., Hesselberth, M., Porcu, M. & Aarts, J. Long-range supercurrents through half-metallic ferromagnetic CrO_2. *Phys. Rev. B* **82**, 100501(R) (2010).

[18] Robinson, J. W. A., Witt, J. D. S. & Blamire, M. G. Controlled Injection of Spin-Triplet Supercurrents into a Strong Ferromagnet. *Science* **329**, 59 (2010).

[19] Khaire, T. S., Khasawneh, M. A., Pratt, W. P., Jr. & Birge, N. O. Observation of Spin-Triplet Superconductivity in Co-Based Josephson Junctions. *Phys. Rev. Lett.* **104**, 137002 (2010).

[20] Sprungmann, D., Westerholt, K., Zabel, H., Weides, M. & Kohlstedt, H. Evidence for triplet superconductivity in Josephson junctions with barriers of the ferromagnetic Heusler alloy Cu_2MnAl. *Phys. Rev. B* **82**, 060505(R) (2010).

[21] Klose, C., Khaire, T. S., Wang, Y. X., Pratt, W. P., Jr., Birge, N. O., McMorran, B. J., Ginley, T. P., Borchers, J. A., Kirby, B. J., Maranville, B. B. & Unguris, J. Optimization of Spin-Triplet Supercurrent in Ferromagnetic Josephson Junctions. *Phys. Rev. Lett.* **108**, 127002 (2012).

[22] Trifunovic, L. Long-Range Superharmonic Josephson Current. *Phys. Rev. Lett.* **107**, 047001 (2011).

[23] Trifunovic, L., Popović, Z. & Radović, Z. Josephson effect and spin-triplet pairing correlations in SF_1F_2S junctions. *Phys. Rev. B* **84**, 064511 (2011).

[24] Richard, C., Houzet, M. & Meyer, J. S. Superharmonic Long-Range Triplet Current in a Diffusive Josephson Junction. *Phys. Rev. Lett.* **110**, 217004 (2013).

[25] Iovan, A., Golod, T. & Krasnov, V. M. Controllable generation of a spin-triplet supercurrent in a Josephson spin valve. *Phys. Rev. B* **90**. 134514 (2014).

[26] Sellier H., Baraduc C., Lefloch F., & Calemczuk R. Half-Integer Shapiro Steps at the 0?π Crossover of a Ferromagnetic Josephson Junction. Phys. Rev. Lett. 92, 257005 (2004).

[27] Radović, Z., Dobrosavljević-Grujić, L., & Vujičić, B., Coexistence of stable and metastable 0 and π states in Josephson junctions. *Phys. Rev. B* **63**, 214512 (2001).

[28] Blonder, G. E., Tinkham, M. & Klapwijk, T. M. Transition from metallic to tunneling regimes in superconducting microconstrictions: Excess current, charge imbalance, and supercurrent conversion. *Phys. Rev. B* **25**, 4515 (1982).

[29] Furusaki, A. & Tsukada, M. Dc Josephson effect and Andreev reflection. *Solid State Commun.* **78** 299 (1991).

[30] Zheng, Z. M. & Xing, D. Y. Josephson supercurrent with spin-equal pairing through a half-metallic link. *J. Phys.: Condens. Matter* **21**, 385703 (2009).

[31] Tanaka, Y. & Kashiwaya, S. Theory of Josephson effects in anisotropic superconductors. *Phys. Rev. B* **56**, 892 (1997).

[32] de Gennes, P. G. Superconductivity of Metals and Alloys. Chapt. 5 (Benjamin, New York, 1966).

[33] Ketterson, J. B. & Song, S. N. Superconductivity, Part III (Cambridge University Press, 1999).

[34] Halterman, K., Valls, O. T. & Barsic, P. H. Induced triplet pairing in clean s-wave superconductor/ferromagnet layered structures. *Phys. Rev. B* **77**, 174511 (2008).

[35] Houzet, M. & Buzdin, A. I. Long range triplet Josephson effect through a ferromagnetic trilayer. *Phys. Rev. B* **76**, 060504(R) (2007).

[36] Meng, H., Wu, X. Q. & Zheng, Z. M. Long-range triplet Josephson current modulated by the interface magnetization texture. *Europhys. Lett.* **104** 37003 (2013).

[37] Visani, C., Sefrioui, Z., Tornos, J., Leon, C., Briatico, J., Bibes, M., Barthélémy, A, Santamaría, J., Villegas, J. E. Equal-spin Andreev reflection and long-range coherent transport in high-temperature superconductor/half-metallic ferromagnet junctions. *Nature Physics* **8**, 539 (2012).

[38] Jin, L. J., Wang, Y., Wen, L., Zha, G. Q. and Zhou, S. P. Spin-triplet current in half metal/conical helimagnet/superconductor heterojunctions. *Phys. Lett. A* **376**, 2435 (2012).

[39] Landau, L. D. & Lifshitz, E. M. Quantum Mechanics, Non-Relativistic Theory, third edition (Pergamon, Elmsford, NY, 1977)

Author contributions

H.M. and J.S.W. conceived the research and performed the calculations. All authors contributed to discussion and reviewed the manuscript.

Additional information

Competing financial interests: The authors declare no competing financial interests.

Figure legends

Figure 1: **Schematic illustration of the $S/F_1/F_2/S$ Josephson junction containing a bilayer ferromagnet.** Thick arrows in F_1 layer and F_2 layer indicate the directions of the magnetic moments. The phase difference between the two s-wave Ss is $\phi = \phi_R - \phi_L$.

Figure 2: **Critical current as a function of the orientation angle (θ_2, φ_2) of the F_2 layer.** Here we set $k_F L_1 = 200$, $k_F L_2 = 6$, $h_1/E_F = 0.1$, and $h_2/E_F = 0.16$.

Figure 3: **The spin-triplet pair amplitudes f_0 and f_1 plotted as a function of the coordinate $k_F y$ for several values of θ_2 in the case of $\varphi_2 = 0$.** The left panels show the real parts while the right ones show the imaginary parts. The dotted vertical lines represent the location of the S/F_1, F_1/F_2 and F_2/S interfaces. Here $k_F L_1 = 200$, $k_F L_2 = 6$, $h_1/E_F = 0.1$, $h_2/E_F = 0.16$, $\omega_D t = 4$, and $\phi = 0$. All panels utilize the same legend.

Figure 4: (a) the Josephson current-phase relation $I_e(\phi)$ for four values of the relative angle θ_2 between magnetizations. (b) The normalized LDOS in the F_1 layer ($k_F y = 180$) plotted versus the dimensionless energy ϵ/Δ for different θ_2, and the results are calculated at $k_B T = 0.0008$. Other parameters are the same as in Fig. 3.

Figure 5: **The x (top panels) and z components (bottom panels) of the local magnetic moment plotted as a function of the coordinate $k_F y$ for different θ_2.** The left panels show the behaviours over the extended F_1 regions while the right ones show the detailed behaviours in the F_2 layer. Other parameters are the same as in Fig. 3.

Figure 6: **The spin-triplet pair amplitudes f_1 [(a) and (b)] and f_2 [(c) and (d)] plotted as a function of the coordinate $k_F y$ for several values of φ_2 in the case of $\theta_2 = \pi/2$.** The left panels [(a) and (c)] show the real parts while the right ones [(b) and (d)] show the imaginary parts. Other parameters are the same as in Fig. 3.

Figure 7: **The x (top panels) and y components (bottom panels) of the local magnetic moment plotted as a function of the coordinate $k_F y$ for different φ_2.** The left panels show the behaviours over the extended F_1 region while the right ones show the detailed behaviours in the F_2 region. Other parameters are the same as in Fig. 3.

Figure 8: Critical current (a) as a function of $k_F L_2$ and θ_2 for $h_2/E_F = 0.16$, and (b) as a function of h_2/E_F and θ_2 for $k_F L_2 = 6$. We set $k_F L_1 = 200$, $h_1/E_F = 0.1$, and $\varphi_2 = 0$.

Figure 9: **Critical current as a function of h_1/E_F and $k_F L_1$.** We set $k_F L_2 = 6$, $h_2/E_F = 0.16$, $\theta_2 = \pi/2$, and $\varphi_2 = 0$.

Figure 10: The imaginary parts of f_0 (a), f_1 (b), $f_{\uparrow\uparrow}$ (c) and $f_{\downarrow\downarrow}$ (d) plotted as a function of the coordinate $k_F y$ for several h_1/E_F. We set $k_F L_1 = 200$, $k_F L_2 = 6$, $h_2/E_F = 0.16$, $\theta_2 = \pi/2$, $\varphi_2 = 0$, $\omega_D t = 4$, and $\phi = 0$.

Figure 11: **Two types of transference about the pairs of correlated electrons and holes.** (a) The first one consists of two normal Andreev reflections occurred at S/F_1 interface and two anomalous Andreev reflections at F_2/S interface in the case of weak exchange field in the F_1 layer. (b) The second one consists of two normal reflections at S/F_1 interface and two anomalous Andreev reflections at F_2/S interface while the F_1 layer is converted into half-metal.

Figure 12: (a) the Josephson current-phase relation $I_e(\phi)$ for different h_1/E_F. (b) The normalized LDOS in the F_1 layer ($k_F y = 180$) plotted versus the dimensionless energy ϵ/Δ, and the results are calculated at $k_B T = 0.0008$. Other parameters are the same as in Fig. 10.

Figure 13: **The x (top panels) and z components (bottom panels) of the local magnetic moment plotted as a function of the coordinate $k_F y$ for different h_1/E_F.** The left panels show the behaviours over the extended F_1 region while the right ones show the detailed behaviours in the F_2 layer. Other parameters are the same as in Fig. 10.